IEEE Access
Multidisciplinary | Rapid Review | Open Access Journal

Received March 20, 2018, accepted April 14, 2018, date of publication April 24, 2018, date of current version May 16, 2018.

Digital Object Identifier 10.1109/ACCESS.2018.2829701

Design of an Energy Management Strategy for a Parallel Hybrid Electric Bus Based on an IDP-ANFIS Scheme

XIANG TIAN[1], REN HE[1], AND YIQIANG XU[2]
[1]School of Automotive and Traffic Engineering, Jiangsu University, Zhenjiang 212013, China
[2]Suzhou Higer New Energy Automobile Electronic Control System Co., Ltd., Suzhou 215121, China

Corresponding author: Xiang Tian (auzn0009@163.com)

This work was supported in part by the Natural Science Foundation of Jiangsu Higher Education Institutions of China under Grant 13KJA580001 and in part by the Priority Academic Program Development of Jiangsu Higher Education Institutions.

ABSTRACT A critical challenge in the energy management of hybrid electric vehicles is how to intelligently distribute the power between engine and electric motor with a significant reduction in fuel consumption and emissions. In this paper, iterative dynamic programming (IDP) and adaptive neurofuzzy inference system (ANFIS)-based energy management strategy was proposed for a parallel hybrid electric bus. First, IDP was used to obtain the optimal control trajectories for a specific driving cycle. During the iterative process, a modified gear-shifting strategy was introduced to achieve a good tradeoff between the fuel economy and the drivability performance. Next, multi-ANFIS networks were designed and trained to learn the control law from the available optimal trajectories. Finally, the real-time energy management controller based on the IDP-ANFIS was built to coordinate the output of the two power sources, which reduces the fuel consumption and emissions. The simulation and experimental results reveal that the IDP-ANFIS is feasible, and the performance is superior to that of the equivalent consumption minimization strategy and rule-based method.

INDEX TERMS Energy management strategy, fuel consumption, iterative dynamic programming, ANFIS, parallel hybrid electric bus.

I. INTRODUCTION

With increasing environmental pollution, global warming and petroleum consumption, the development of new energy vehicles has received considerable attention [1]–[4]. Hybrid electric vehicles (HEVs) equipped with an engine and an electric motor is a practical and economical solution to alleviate the above mentioned problems during the short term. Compared with conventional vehicles, HEVs with multiple power paths have the potential to significantly reduce fuel consumption and emissions [5]–[9]. The power distribution between the different power sources, which is determined by an energy management strategy (EMS), is one of the crucial factors affecting the vehicle performance. Therefore, optimizing the EMS to achieve optimal fuel economy and emissions is an important task for HEVs development.

It is well known that the function of an EMS is to determine the optimal power distribution, which ensures that the vehicle is in a suitable operating mode under different driving conditions [10]. In addition, the condition of charge-sustainability can be regarded as a constraint, imposing a zero deviation in the battery state of charge (SOC) over the driving cycle. Currently, many control methods have been proposed for HEVs to optimize the EMS. A classical rule-based EMS whose logical rules are 'if-then' type is widely used in the early stages [11], [12]. This method with a strong real-timeliness and good reliability is easy to implement in practice. However, the rules design depends on the engineers' experience and experimental data. In [13] and [14], a fuzzy algorithm is introduced to realize an online and suboptimal power distribution for series HEV instead of using heuristics rules. Actually, this is only an extension of the rule-based EMS. To obtain an optimal EMS, Pérez *et al*. [15] proposed a dynamic programming (DP) approach to solve the power distribution problem for a parallel HEV. However, this approach is impossible in reality, since it requires the entire driving condition to be known in advance. To overcome this issue, a new rule-based strategy whose rules are derived from DP results is proposed by Bianchi *et al*. [16] for a series-parallel HEV.

An obvious reduction of the computational time can be easily achieved during its online implementation. Some researchers focused on using the state transfer matrix of the driver's power demand to predict the future power demand sequence. Lin *et al*. [17] proposed a stochastic dynamic programming to generate the control law, which can be implemented online . However, the state transition probabilities are associated with the driving cycles, which may severely worsen the computational burden. The equivalent consumption minimization strategy (ECMS) is a powerful online approach to reduce fuel consumption in a hybrid system, as initially presented by Paganelli *et al*. [18] . The equivalent factor is introduced to weight the electrical power in [19] and [20], and it represents the conversion relation from electricity consumption into equivalent fuel consumption. With appropriate regulation of the equivalent factor, the ECMS can generate results close to the optimum. In [21], a particle swarm optimization algorithm is used to optimize the equivalent factor at each segment of the specific cycle, and a 2-dimensional table regarding the optimum factor is obtained for realizing a real-time adaptive EMS for plug-in parallel HEV. Musardo *et al*. [22] developed an adaptive ECMS for a parallel HEV that can estimate the equivalent factor through an on-the-fly algorithm according to the trip information . However, these algorithms with adaptive tuning of the factor are the lack of the capability of reasoning and learning, which are very sensitive to the driving cycle information. Furthermore, a model predictive control method is introduced to devise the EMS for a parallel HEV that can obtain a reasonable power distribution [23].

As mentioned above, many intelligent algorithms have been used to design the EMS for HEVs. Among them, dynamic programming, as a global optimization technique, is suitable to obtain the optimal EMS through a recursive calculation. Considering the limitation of online application for the dynamic programming, this paper presents an innovative approach to design the EMS for a parallel hybrid electric bus. First, due to the regular and relative fixed route of a city bus, the energy management control problem can be formulated as a nonlinear optimization problem with hard constraints over a specific driving cycle. The cost function is concerned within three parts, i.e., fuel consumption, emissions and battery SOC. To avoid the phenomena of the dimensionality curse, iterative dynamic programming (IDP) is employed to solve the above optimization problem using coarse grids and a multistep iterative strategy, which ensures the calculation accuracy. Meanwhile, the optimization process should take the gear-shifting strategy correction into consideration to maintain the vehicle dynamic performance. Therefore, an adaptive factor λ is applied to correct the gear-shifting strategy, whose value is determined by the fuzzy control algorithm. Finally, an adaptive neuro-fuzzy inference system (ANFIS) is applied to set up a real-time energy management controller, and the optimal control trajectories produced by IDP approach are taken as the training data. Taking advantage of both the fuzzy system for its reasoning capability and neural network for its learning capability, the multi-ANFIS networks have a superior ability to extract the control law from the optimal trajectories. The simulations and experiments results are evaluated to reveal the advantage of proposed method in fuel economy and emissions improvement.

This paper is organized as follows. In the next section, a model of the parallel hybrid electric bus is described, and Section III presents the IDP-based EMS step by step. Then, the obtained results form the foundation for the real-time energy management controller discussed in Section IV. The control results are revealed in Section V where the performance is represented in terms of fuel consumption and emissions. Finally, the conclusions are presented in Section VI.

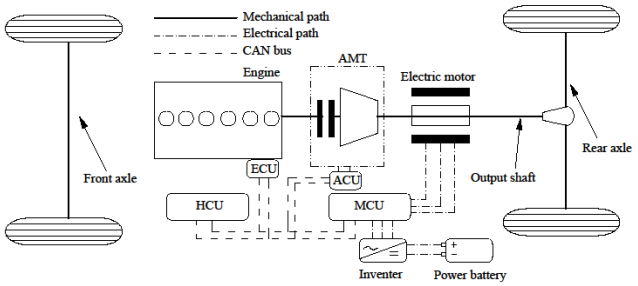

FIGURE 1. Configuration of the parallel hybrid electric bus.

II. HYBRID POWERTRAIN MODEL

A. VEHICLE POWERTRAIN CONFIGURATION

This section outlines a parallel hybrid electric bus studied in this paper. The configuration is shown in Fig. 1, which consists of an engine, an electric motor and an automated mechanical transmission (AMT). The AMT is located on the same axis between the engine and the electric motor. The electric motor is mechanically connected to the drive shaft, then the regeneration of braking energy with high-efficiency becomes possible. Table 1 lists main parameters of the powertrain components.

TABLE 1. Main parameters of powertrain components.

	Item	value
Engine	Rated power (kW)	147
	Rated speed (rpm)	2500
	Max. Torque (N.m)	710
Electric motor	Rated power (kW)	100
	Rated speed (rpm)	1600
	Max. Torque (N.m)	2800
AMT	Gear ratios	4.763/2.808/1.594/1.00/0.756
Battery	Energy Capacity (kW.h)	26.6
	Rated voltage (V)	384

B. VEHICLE MATHEMATICAL MODELS

To analyze the internal energy flow and model the energy management of the hybrid system, it is necessary to build the models of the critical powertrain components. Due to the complexity of the components, the modeling method combining experimental data and theoretical analysis is applied in

this section. Obviously, all of the component models can be integrated to form the entire system model. The optimization of the EMS for the hybrid electric bus is also based on this system model.

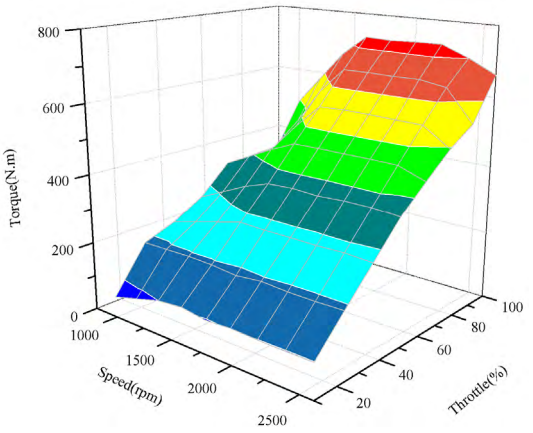

FIGURE 2. The engine torque characteristic map.

1) ENGINE MODEL

Due to the nonlinear characteristics, the engine model can be established based on experimental data. The engine torque characteristic map is shown in Fig. 2. Considering the time delay in the dynamic response of the engine, a first-order inertia transfer function with time constants τ_e is introduced. The engine torque can be written as

$$T_e = \frac{1}{1+\tau_e s} f\left(\omega_e, \alpha_e\right) \tag{1}$$

where T_e and ω_e represent the engine torque and speed, respectively, and α_e is the throttle opening. Note that the throttle opening is provided by the vehicle control unit (VCU) in practice.

Then, the engine fuel consumption and emissions can be calculated by using a lookup table or fitting parameters. The relevant data are acquired from the engine bench test. Therefore, the model of fuel consumption and emissions are expressed as

$$\dot{m}_f = f_{fuel}\left(T_e, \omega_e\right) \tag{2}$$

$$b_{CO} = \overline{BS_{CO}}\left(T_e, \omega_e\right) \tag{3}$$

$$b_{HC} = \overline{BS_{HC}}\left(T_e, \omega_e\right) \tag{4}$$

$$b_{NO_x} = \overline{BS_{NO_x}}\left(T_e, \omega_e\right) \tag{5}$$

where $\dot{m}_f$ is the brake specific fuel consumption; b_{CO}, b_{HC} and b_{NO_x} represent the brake specific emission of CO, HC, and NO_x, respectively. The engine BSFC map is presented in Fig. 3.

2) ELECTRIC MOTOR MODEL

An electric motor has two modes, motoring mode (electric motor) and generating mode (electric generator). While the electric motor operates in the generating mode, the chemical energy or braking energy can be converted into electric

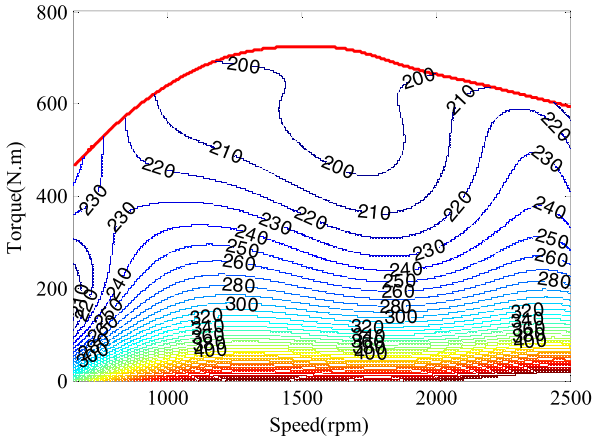

FIGURE 3. The engine BSFC map.

energy and stored in the battery. In this section, an electric motor model with an efficiency modeling method is constructed, and the electric motor torque T_m is obtained by

$$T_m = \frac{1}{1+\tau_m s} \min\left(T_{md}, \frac{P_{max}}{9549\omega_m}\right) \tag{6}$$

$$P_m = \begin{cases} \dfrac{T_m\omega_m}{\eta_m}, & (T_m \geq 0) \\ T_m\omega_m\eta_m, & (T_m < 0) \end{cases} \tag{7}$$

$$I_m = \frac{P_m}{V_B} \tag{8}$$

where ω_m, P_m and I_m are the speed, power and current of the electric motor, respectively. η_m and τ_m are the efficiency and time constant for the electric motor, respectively. T_{md} and P_{max} are the command torque and peak power, respectively. V_B is the DC bus voltage. The electric motor efficiency model is shown in Fig. 4.

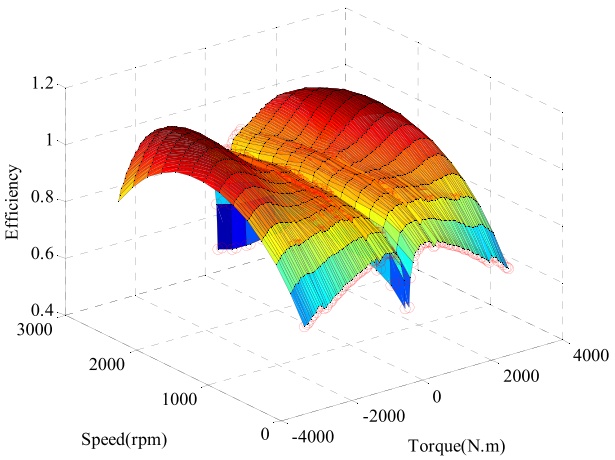

FIGURE 4. The electric motor efficiency model.

3) BATTERY MODEL

The battery functions as a secondary energy source to stimulate the electric motor and regenerate the braking energy.

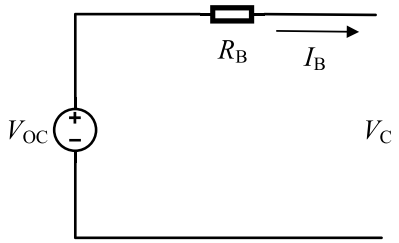

FIGURE 5. The equivalent circuit model of the battery.

Considering the complex chemical reaction inside the battery, an equivalent circuit model is adopted in this study. As shown in Fig. 5, the equivalent circuit model contains an ideal voltage source and an internal resistance, both of which are affected by the temperature and SOC. The power of the battery P_B can be expressed as

$$P_B = V_C I_B \tag{9}$$

where V_C and I_B are the terminal voltage and charge/discharge current of the battery, respectively. On the basis of Kirchhoff's voltage law, the terminal voltage of the battery can also be defined as

$$V_C = V_{OC} - I_B R_B \tag{10}$$

According to (9) and (10), the charge/discharge current of the battery I_B can be rewritten as

$$I_B = \frac{V_{OC}}{2R_B} - \sqrt{\left(\frac{V_{OC}}{2R_B}\right)^2 - \frac{P_B}{R_B}} \tag{11}$$

where R_B and V_{OC} are the internal resistance and open-circuit voltage of the battery, respectively. The current battery SOC can be derived by the ampere hour algorithm shown as

$$soc = \frac{1}{Q_I}\left(Q_0 - \frac{1}{3600}\int_0^t I_B dt\right) \tag{12}$$

where Q_0 and Q_I represent the initial and total capacity of the battery, respectively.

4) AMT MODEL

For the AMT, both the clutch operation and gear selection are automatically controlled by the control unit according to the predefined procedure. However, the clutch torque with nonlinear characteristics influences the vehicle drivability during the slipping phase. The dynamics of the clutch can be expressed as

$$T_c = \begin{cases} 0, & \text{unlock} \\ \dfrac{2N_c u_c \left(R^3 - r^3\right) P_c \mathrm{sgn}\left(\Delta\omega\right)}{3\left(R^2 - r^2\right)}, & \text{slip} \\ T_i, & \text{lock} \end{cases} \tag{13}$$

where T_c is the torque transferred by the clutch, T_i is the AMT input shaft torque, u_c is the friction coefficient of the friction plate, N_c is the number of friction plates, P_c is the pressure of cylinder used to manipulate the disengagement or engagement of the clutch. R and r are the outer and inside radius of the diaphragm spring, respectively. $\Delta\omega$ denotes the speed difference between the two sides of the clutch.

The AMT consists of two statuses, i.e., the engaged and neutral statuses. When the AMT is in a neutral status, the engine torque is isolated from the hybrid powertrain. Therefore, the output torque of the AMT can be expressed as

$$T_a = \begin{cases} 0, & \text{neutral status} \\ T_c i_g\left(n\right), & \text{engaged status} \end{cases} \tag{14}$$

where $i_g(n)$ represents the current gear ratio.

III. ITERATIVE DYNAMIC PROGRAMMING-BASED ENERGY MANAGEMENT STRATEGY

For a parallel HEV, energy management is a global optimization problem whose objective is to determine the power distribution between engine and electric motor, minimizing fuel consumption and emissions [24]. As well known, the engine operating points should be concentrated in the high efficiency region as much as possible, so that a sound fuel economy can be achieved. Alternatively, the supernumerary dynamic energy of the vehicle must be used to charge the battery to improve the system energy efficiency. Moreover, the state variables and control variables must satisfy the constraints that are determined by the normal operation range of the powertrain components. Hence, the energy management of the hybrid electric bus can be converted into a class optimal control problem with hard constraints, and its discrete-time form is defined as

$$\begin{cases} \min\ J = \sum_{i=k_0}^{N} L\left[x\left(i\right), u\left(i\right), i\right] \\ x\left(k+1\right) = f\left[x\left(k\right), u\left(k\right), k\right], \quad k \in \left[k_0, N\right] \end{cases}$$
$$S.t. \begin{cases} x\left(k_0\right) = x_0 \\ x_{\min} \le x\left(k\right) \le x_{\max} \\ u_{\min} \le u\left(k\right) \le u_{\max} \end{cases} \tag{15}$$

where J is the cost function, L is the instantaneous cost value, $u(k)$ and $x(k)$ are control and state vectors, respectively, and x_0 is the initial value of the state vector.

A. ENERGY MANAGEMENT IN THE HYBRID ELECTRIC BUS MODELING

Based on the vehicle configuration shown in Fig. 1, the relationship between the coupling torque produced by the two power sources and the drive torque can be formulated as

$$T_w = \left[T_e \cdot i_g\left(n_{AMT}\right) + T_m\right] i_0 \eta_T \tag{16}$$

where T_w is the drive torque (acting on the wheel), T_e and T_m are the engine and electric motor torque, respectively, η_T is the transmission efficiency, i_0 and $i_g(n_{AMT})$ are the gear ratio of the final drive and AMT, respectively. According to the vehicle dynamics equation, the drive torque can also be

expressed as

$$T_{\mathrm{w}} = \sum F \cdot r_{\mathrm{w}} = \left(mgf_{\mathrm{r}} \cos\theta + mg \sin\theta + \frac{1}{2} C_D A \rho v^2 + \delta m \frac{dv}{dt} \right) \cdot r_{\mathrm{w}} \tag{17}$$

where r_{w} is the wheel radius, m, g, θ and f_{r} denote the vehicle mass, gravity acceleration (9.8 m/s^2), road slope and rolling friction coefficient, respectively. v, ρ, C_{D} and A denote the velocity, air density, air drag coefficient and frontal area, respectively. δ is the equivalent moment of inertia.

Once the vehicle acceleration is determined, the drive torque of the vehicle can be assumed by (17) in advance. Thus, only two variables should be chosen from (16) as the control variables because of the causation relations between them. Accordingly, the commands of the electric motor torque and gear shifting are regarded as the control variables. Besides, the accelerator pedal travel, brake pedal travel, vehicle velocity, battery SOC and current gear status are used as the input signals of the vehicle control unit. The independent signals among them, including battery SOC and current gear status, are taken as state variables. Consequently, the state vector and control vector at phase k are defined as

$$\begin{cases} x(k) = \{n_{\mathrm{AMT}}(k), soc(k)\} \\ u(k) = \{n_{\mathrm{AMT\_cmd}}(k), T_{\mathrm{m\_cmd}}(k)\} \end{cases} \tag{18}$$

where soc represents the battery SOC, $T_{\mathrm{m\_cmd}}$ is the torque command of the electric motor, and $n_{\mathrm{AMT\_cmd}}$ and n_{AMT} are the gear shifting command and current gear, respectively.

Note that the optimization process for the power distribution must take consider the deviation in the battery SOC over the entire cycle. The SOC balance problem is presented as a hard constraint, which achieves a fair comparison between different methods in simulation and avoids battery depletion in real driving situation. Hence, the penalty function is introduced, and the cost function is given by

$$J = \sum_{k=1}^{M} \left\{ \int_{t_{k-1}}^{t_k} L_{\mathrm{C}}[x(t), u(t), t]\, dt + \alpha |b_{\mathrm{CO}}(k) - B_{\mathrm{CO}}| + \beta |b_{\mathrm{HC}}(k) - B_{\mathrm{HC}}| + \chi \left| b_{\mathrm{NO_x}}(k) - B_{\mathrm{NO_x}} \right| \right\} + \delta [soc(M) - soc(0)]^2 \tag{19}$$

where M is the number of time stages. L_{C} represents the fuel consumption function. $\mathrm{B_{CO}}$, $\mathrm{B_{HC}}$ and $\mathrm{B_{NOx}}$ represent the desired values for the brake specific emissions of CO, HC and $\mathrm{NO_x}$, respectively. α, β, χ and δ are the weighting factors for the corresponding terms. Moreover, some constraints are fulfilled due to the operating range of the powertrain components. The constraints are shown as

$$\begin{cases} soc_{\min} \le soc(k) \le soc_{\max} \\ \omega_{\mathrm{e,min}} \le \omega_e(k) \le \omega_{\mathrm{e,max}}, \quad T_{\mathrm{e,min}} \le T_e(k) \le T_{\mathrm{e,max}} \\ \omega_{\mathrm{m,min}} \le \omega_m(k) \le \omega_{\mathrm{m,max}}, \quad T_{\mathrm{m,min}} \le T_m(k) \le T_{\mathrm{m,max}} \end{cases} \tag{20}$$

where $T_{\mathrm{e}}(k)$, $\omega_{\mathrm{e}}(k)$, $T_{\mathrm{m}}(k)$, $\omega_{\mathrm{m}}(k)$, $soc(k)$ and represent the engine torque, engine speed, electric motor torque, electric motor speed and battery SOC at phase k, respectively.

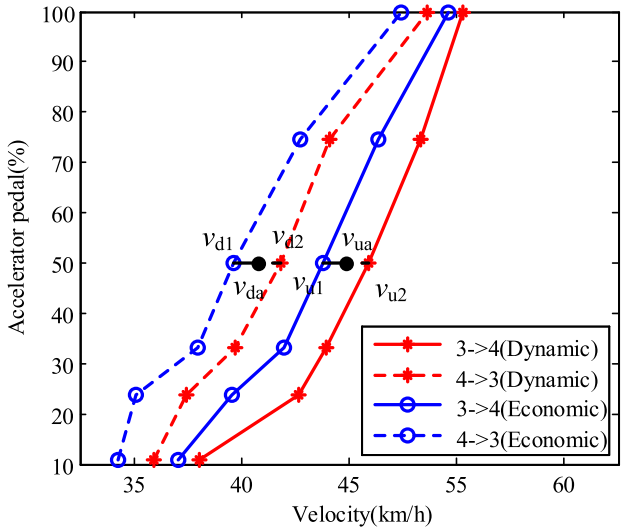

FIGURE 6. Gear-shifting curves of the economy and dynamic schedule.

B. GEAR-SHIFTING STRATEGY CORRECTION

In this study, the gear-shifting strategy is mapped as a lookup table of the vehicle velocities and pedal accelerations, as shown in Fig. 6. The gear-shifting logic between 3 and 4 is taken as an example. The gear-shifting strategy, divided into the economic and dynamic modes, is applied to obtain the different performance. From Fig. 6, it can be observed that the economical gear-shifting strategy tends to downshift later and upshift earlier in comparison with that of the dynamic gear-shifting strategy. Thus, the economical gear-shifting strategy ensures an obvious improvement in the fuel economy, while the vehicle drivability apparently deteriorated [25]. In addition, the same is true for the dynamic gear-shifting strategy. The economical gear-shifting strategy will be selected to obtain the best fuel economy, which results in the deterioration in the drivability performance. To solve this issue, an adaptive factor λ is introduced to correct the gear-shifting strategy for achieving a good tradeoff between the fuel economy and the drivability performance. The modified gearshift points (the upshift point v_{ua} and the downshift point v_{da}) can be defined as

$$\begin{cases} v_{\mathrm{ua}} = (1-\lambda) v_{\mathrm{u1}} + \lambda v_{\mathrm{u2}} \\ v_{\mathrm{da}} = (1-\lambda) v_{\mathrm{d1}} + \lambda v_{\mathrm{d2}}, \end{cases} \quad \lambda \in [0, 1] \tag{21}$$

where v_{u1} and v_{u2} represent the economic and dynamic upshift points, respectively. The parameters v_{d1} and v_{d2} represent the economic and dynamic downshift points, respectively. The adaptive factor $\lambda = 1$ represents the economical gear-shifting strategy, and $\lambda = 0$ represents the dynamic gear-shifting strategy.

In practice, the driver's intention can be reflected by a variation in the accelerator pedal. It is indicated that a large

variation in the accelerator pedal in a short time is the goal for vehicle drivability. Similarly, a small variation is the goal for vehicle fuel economy. Alternatively, the influence of vehicle acceleration on the gear selection of the AMT cannot be ignored. Thus, the vehicle acceleration (a_{veh}) and rate of change in the accelerator pedal (α_{ap}) are two critical parameters to determine the gear selection. In this study, fuzzy logic control (FLC) is applied to obtain the value of the adaptive factor for modifying the gear-shifting strategy according to the driver's intention. The aforementioned parameters with a normalized value of [0, 1] are set as the input variables of the FLC, and the adaptive factor λ is set as the output variable. The membership functions (MFs) of the FLC input variables and output variable are shown in Fig. 7. As shown, the 'S', 'M', and 'B' represent the small, medium and big input value, respectively. The 'S', 'MS', 'MB', and 'B' represent the small, medium-small, medium-big and big output value, respectively. The FLC rules are shown in Table 2.

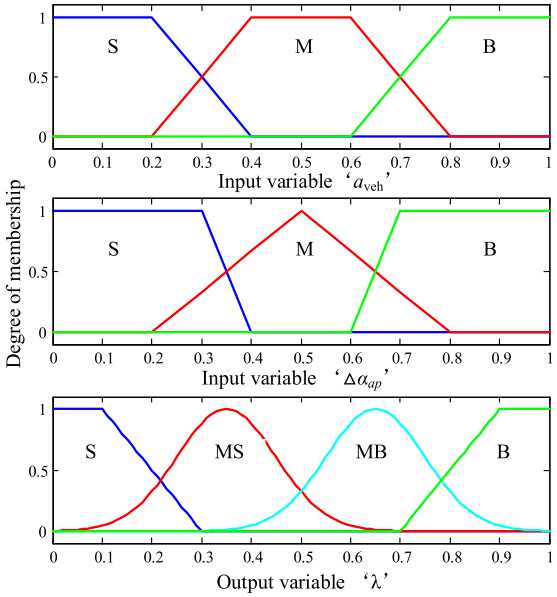

FIGURE 7. The membership functions (MFs) of the FLC.

TABLE 2. Fuzzy rules of the FLC.

Condition number	If $\Delta\alpha_{\text{ap}}$	And a_{veh}	Then λ
1	B	B	S
2	B	M	S
3	B	S	MS
4	M	B	MB
5	M	M	MS
6	M	S	MB
7	S	B	MB
8	S	M	B
9	S	S	B

Based on these definitions, the FLC is devised to dynamically adjust the value of λ, and the block diagram of FLC is shown in Fig. 8. As is well known, the center of the gravity method is widely utilized for defuzzification in many areas [26]. This method is also selected to apply in this study,

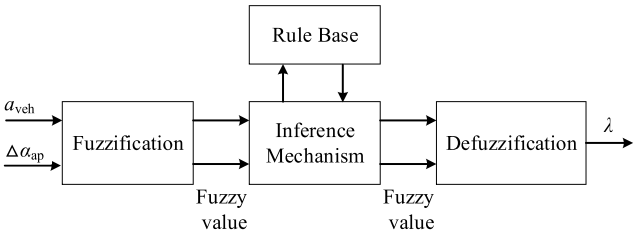

FIGURE 8. The block diagram of FLC.

and it can be expressed as

$$u = \frac{\sum_i g_i \int u_i}{\sum_i \int u_i} \tag{22}$$

where u denotes the output value, g_i represents the center of the MFs as a consequence of the rules and u_i is the value of i^{th} output level.

Here, the accelerator pedal α_{ap} can be determined by

$$\alpha_{\text{ap}} = \frac{T_{\text{w}} \cdot K_{\text{md}}(soc)}{T_{\text{tol\_m}} \cdot i_0} \tag{23}$$

where $T_{\text{tol\_m}}$ denotes the modified total torque and $K_{\text{md}}(soc)$ is the correction factor as a look-up table function of the battery SOC. The correction factor $K_{\text{md}}(soc)$ is related to the accelerating performance of the vehicle. When the battery SOC is low, the discharging trend is suppressed and this results in a decline of motor torque. Hence, this correction factor is applied to dynamically adjust the parameter α_{ap} on the basis of battery SOC. In Fig. 9, the curve with the purple color represents the maximum torque of the electric motor, and the curve with the green color represents the maximum torque of the engine at the output side of the AMT.

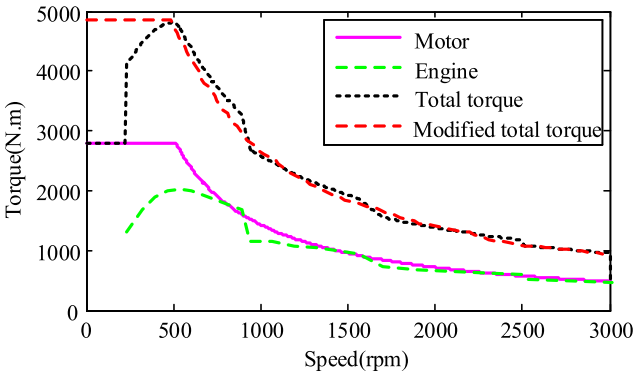

FIGURE 9. The total torque at output side of the AMT.

C. SOLUTION OF THE ENERGY MANAGEMENT FOR THE HYBRID ELECTRIC BUS

Compared with conventional approaches, dynamic programming method can generate a globally optimal policy using the recursive calculation, and it is suitable to address the complex, nonlinearity and constraint problems. However, the accuracy of the DP method is based on fine grids for variables. For high dimensional problems, the DP method requires very

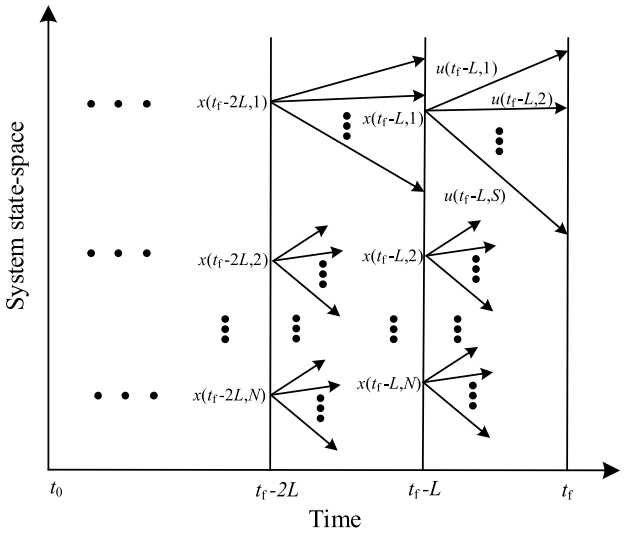

FIGURE 10. Illustration of the iterative dynamic programming algorithm.

large amounts of memory space and calculation time, which results in the curse of dimensionality. To solve this issue, Luss [27] proposed iterative DP (IDP) method in 1990. The iterative technology is applied to compensate for the error incurred by variables discretization. Even the utilize of relatively coarse girds for variables can also ensure achieving the global optimum. The illustration of the IDP method is shown in Fig. 10, and main steps can be summarized as follows.

Step 1: The time interval $[t_0, t_f]$ is divided into P time stages with the same length L. In addition, the length L can be calculated using

$$L = \frac{t_f - t_0}{P} \tag{24}$$

Step 2: The number of allowable value for control vector u denoted by N is chosen and N is odd. Then, an initial control vector u^0 is set at each time stage. Taking the initial control vector u^0 as the midpoint, N control trajectories are produced at each time stage, represented by

$$\left\{u^0 \pm \left[\frac{H}{N-1}\right] \cdot r^i, H = 0, 2, 4, \cdots, N-1\right\} \tag{25}$$

where r^0 denotes the initial region size, and i represents the iteration number index. Thereafter, $N\times P$-dimensional matrix of the initial control $\boldsymbol{U}_{\mathbf{N}\times\mathbf{P}}$ is available.

Step 3: The initial state vector denoted by x^0 is chosen, and the state vector with $N \times P$ dimensions (grid points for the state vector) is produced by using the matrix $\boldsymbol{U}_{\mathbf{N}\times\mathbf{P}}$, which is integrated in the state equation.

Step 4: Starting at stage P, corresponding to time t_f-L, the performance index is calculated at each grid point for the state vector by using the control vector; the differential equations from t_f–L to t_f is integrated; and the control vector that provides the minimum performance index to store $u(P\text{-}1)$ is selected.

Step 5: After stepping back to stage P-1, corresponding to time t_f-$2L$, the performance index in this stage is calculated. In the event that the resulting state vector is not equal to the above grid points for the state vector, the corresponding control vector is chosen to calculate the performance index in stage P, which is the closest neighbor to the above grid points. Likewise, the control vector that provides the minimum performance index from t_f–$2L$ to t_f is selected to store $u(P\text{-}2)$.

Step 6: The procedure is continued until stage 1, and the best control vector in stage 1 is chosen to store $u(0)$. Hence, the one iteration is completed.

Step 7: The region of the permissible control is reduced by

$$r^{i+1} = (1 - \zeta) \cdot r^i \tag{26}$$

where ζ is the region contraction factor. It is applied to reduce the permissible control region during each iteration. Then, the best control vector from step 6 is used as the midpoint.

Step 8: Increment the iteration index i by 1 and jump to step 2. Continue the procedure for a specified number of iterations and then check results.

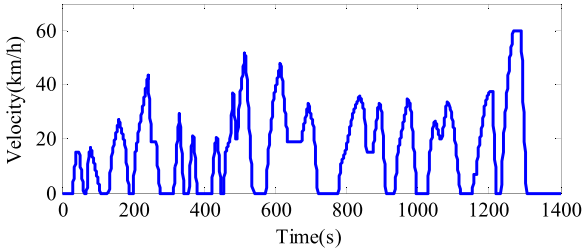

FIGURE 11. The China typical city bus driving cycle.

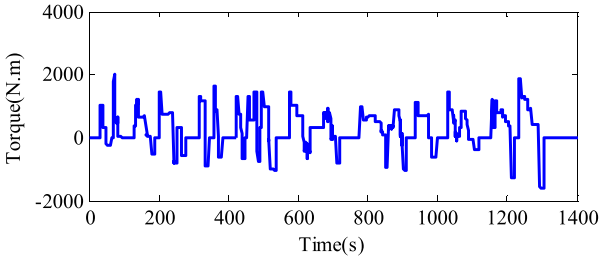

FIGURE 12. The driver torque demand for the CCBC cycle.

As is noted in the preceding context, IDP still employs the inversely recursive calculation to solve the optimal control problem, which relies on prior and complete knowledge of future scenarios. Considering the regularity of city bus routes, vehicle velocity can be gathered in advance. Thus, the optimal EMS for the hybrid electric bus can be obtained by the IDP method. For the sake of simplicity, the China typical city bus driving cycle (CCBC) is selected as the test cycle, as shown in Fig. 11. The driver torque demand for the CCBC cycle is shown in Fig. 12, which can be calculated according to the vehicle parameters as listed in Table 3.

The entire CCBC cycle is discretized to 1315 stages during the calculation process. The grid points for both $n_{\mathrm{AMT\_cmd}}$

TABLE 3. Parameters of the hybrid electric bus.

Parameter	Value
Wheel radius R_w	0.512 m
Vehicle mass M_{veh}	16500 kg
Ratio of the final drive i_0	5.571
Rolling friction coefficient f_r	0.02
Air drag coefficient C_D	0.65
Air density ρ	1.2258 kg/m^3
transmission efficiency η_T	0.9

and n_{AMT} are set to 5. It should be emphasized that zero values for both the n_{AMT_cmd} and n_{AMT} represent the neutral status of the transmission. Otherwise, the transmission is in the engaged status. During the engaged status, the gear status is dependent on the vehicle velocity and pedal acceleration according to the gear-shifting strategy described before. The grid points for both *soc* and T_{m_cmd} are set to 15. The contraction factor is selected to be 0.2, and the initial battery SOC is set to be 0.55.

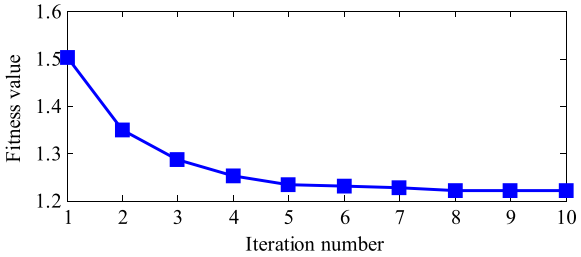

FIGURE 13. The fitness value over the CCBC of each iteration.

Fig. 13 illustrates the fitness value over CCBC of each iteration. After 10th iteration, the fitness value converges to the final value. Compared with the DP method while getting equal accuracy, the number of memory space and computation time requirement for the IDP method are approximately reduced by 7 times and 5 times, respectively. The calculation results of the CCBC cycle are presented in Fig. 14. It can be observed from the figure that the engine and electric motor are coordinated to operate together during the entire cycle. The engine is regulated to operate in a high-efficiency area, and this will result in a reduction in both fuel consumption and emissions. The fuel economy obtained by IDP approach is 24.29 L/100 km, and the HC, CO and NO_x production are 0.005 g/km, 1.612 g/km, and 3.257 g/km, respectively.

IV. REAL-TIME ENERGY MANAGEMENT STRATEGY DEVELOPMENT BASED ON IDP-ANFIS

From Fig. 14, it is derived that the optimal control law from the IDP minimizes the fuel consumption and exhaust emissions. However, the obtained control law is associated with the time horizon, which assumes that the deviation of actual vehicle velocity to the reference value is unchanged. Actually, the above control law cannot be implemented online because of the uncertainty in the state at a definite time. Hence, the ANFIS approach is proposed to fit the offline optimal operating points as the control laws that provide guidance for the real-time control. Taking advantages of both reasoning

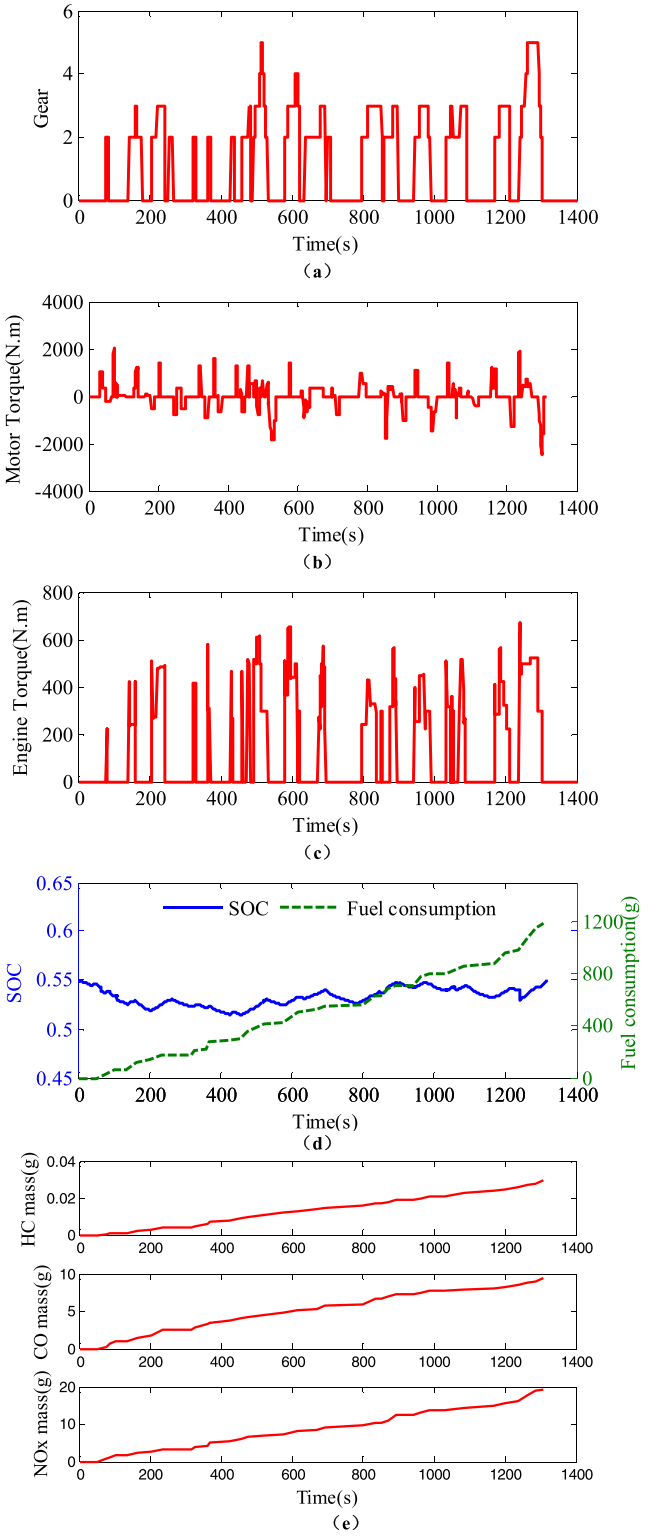

FIGURE 14. Calculation results of the CCBC cycle. (a) Gear. (b) Electric motor torque. (c) Engine torque. (d) Battery SOC and fuel consumption. (e) Emission mass.

capabilities of fuzzy logic and learning capabilities of a neural network, the ANFIS model based on the Sugeno fuzzy inference system is an effective method to model the relationship between the input and target values [28], [29]. The general

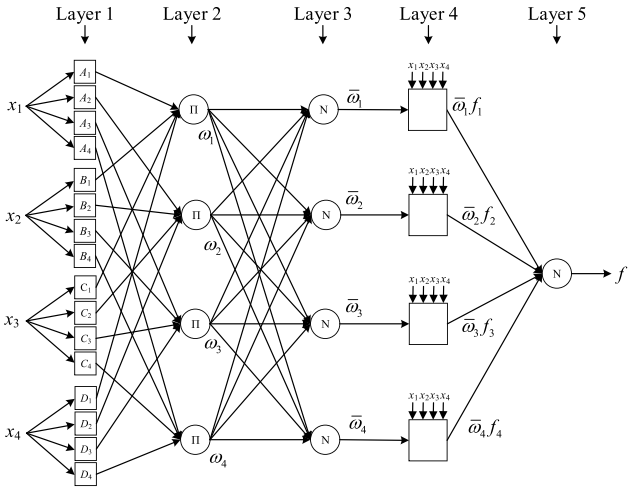

FIGURE 15. The ANFIS general architecture.

ANFIS architecture with four inputs is used to elaborate its basic principle, and the demonstration is illustrated in Fig. 15. As is well known, the fuzzy rules of Sugeno type can be summarized as

Rule i: If x_1 is A_i, x_2 is B_j, x_3 is C_k, and x_4 is D_l,
then $f_i = p_i x_1 + q_i x_2 + r_i x_3 + m_i x_4 + n_i$

where x_1, x_2, x_3 and x_4 are the input of the fuzzy model; f_i denotes the output of the fuzzy model; A_i, B_j, C_k and D_l are the fuzzy sets; p_i, q_i, r_i, m_i and n_i are the consequent parameters.

In fact, the ANFIS is a fuzzy model that is configured in the framework of an adaptive system. This structure achieves the desired performance using learning and adaptation [30]. There are five layers in the ANFIS architecture. The nodes in layers 1 and 5 represent the training and predictive values, respectively. Other nodes in the hidden layers are functioned as the membership functions and fuzzy rules. The parameters in layer 1 called the premise parameters are associated with the input membership function, whereas the parameters in layer 4 correspond to a first-order polynomial. As a result, layers 1 and 4 are the adaptive layers in this structure. The modifiable parameters of layers 1 and 4 can be updated by the learning algorithm to facilitate matching between the ANFIS output and the training data. The output of each layer for the ANFIS can be expressed as [31]

$$\begin{cases} O_i^1 = u_{A_i}(x_1) \\ O_i^2 = \omega_i = u_{A_i}(x_1) \times u_{B_j}(x_2) \times u_{C_k}(x_3) \times u_{D_l}(x_4) \\ O_i^3 = \bar{\omega}_i = \dfrac{\omega_i}{\sum_{j=1}^{i} \omega_i} \\ O_i^4 = \bar{\omega}_i f_i = \bar{\omega}_i (p_i x_1 + q_i x_2 + r_i x_3 + m_i x_4 + n_i) \\ O_i^5 = f = \sum_{i=1}^{j} \bar{\omega}_i f_i = \dfrac{\sum_i \omega_i f_i}{\sum_i \omega_i} \end{cases} \tag{27}$$

where O_i^1, O_i^2, O_i^3, O_i^4 and O_i^5 represent the output values for the i^{th} node in layers 1, 2, 3, 4 and 5, respectively. The parameters u_{A_i},u_{B_j}, u_{C_k} and u_{D_l} represent the membership function of the linguistic label A_i, B_j, C_k and D_l, respectively. ω_i denotes the firing strength of a rule for the i^{th} node and $\bar{\omega}_i$ denotes the normalized firing strength for the i^{th} node.

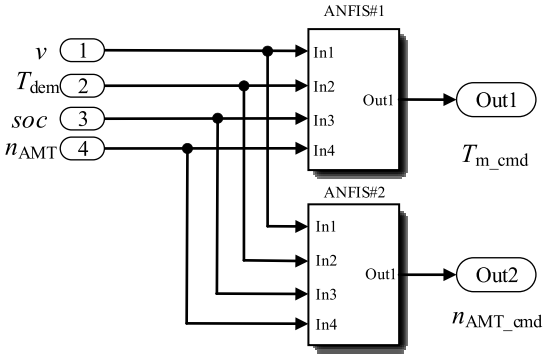

FIGURE 16. The multi-ANFIS model for real-time energy management of the hybrid electric bus.

TABLE 4. The pass way for the ANFIS.

	Forward pass	Backward pass
Signals	Node outputs	Error signals
Consequent parameters	Least-squares	Fixed
Premise parameters	Fixed	Gradient descent

In this paper, multi-ANFIS networks are used to generate the control law. For each control variable, one ANFIS is dedicated, leading to the architecture of the model as shown in Fig. 16. Note that each ANFIS has the same input including the vehicle velocity v, the driver's demand torque T_{dem}, the battery SOC, and the current gear status n_{AMT}. The output of the ANFIS#1 and ANFIS#2 are the electric motor torque command $T_{\text{m\_cmd}}$ and gear-shifting command $n_{\text{AMT\_cmd}}$, respectively. Here, a hybrid algorithm is selected as the learning algorithm for the ANFIS, which consists of the gradient descent approach and least squares method. The pass way for the ANFIS is listed in Table 4, and the training procedure can be summarized as [32]

1) When the premise parameters are fixed, the consequent parameters are tuned in the forward pass using the least squares method.
2) According to error signals of feedback, the gradient descent approach is applied to update the premise parameters in the backward pass with the fixed consequent parameters.

The available training data sets are chosen from the optimal results derived by the IDP method. Considering the normal operating range for the battery, the data sets with different initial battery SOCs ($soc = 0.45, 0.5, 0.6, 0.65$) are applied to train the ANFIS network, and the data sets with initial battery SOC value of 0.55 are used to cross validate. The error in the aforementioned training can be defined as

$$E = \frac{1}{N} \sum_{k=1}^{N} \left(f_k - f_k'\right)^2 \tag{28}$$

where N is the number of the training data, f_k and f_k' are the desired and predicted values, respectively.

TABLE 5. Performance indices for the models.

Model	Number of training data	Number of validation data	Model error (mean square)	(R^2)
ANFIS #1	5260	1315	0.068	0.946
ANFIS #2	5260	1315	0.093	0.921

Once the training procedure has been completed, the adaptive parameters are determined and remained unchanged. The performance of the designed models is listed in Table 5. The outputs of multi-ANFIS networks sufficiently match the training data. The MSE and R-squared values of the ANFIS#1 are 0.068 and 0.946, respectively. For ANFIS#2, the values correspond to 0.093 and 0.921. It is clear that multi-ANFIS networks with certain parameters can be implemented for real-time energy management control of the parallel hybrid electric bus.

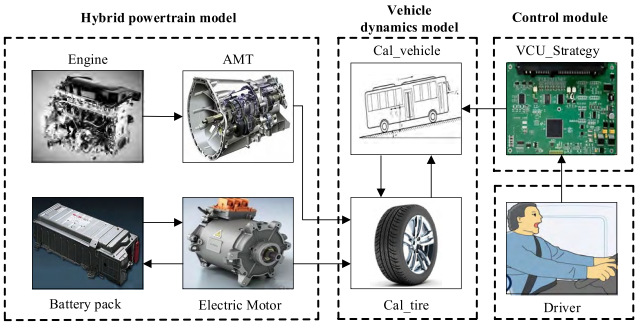

FIGURE 17. The simulation model for the hybrid electric bus.

V. RESULTS AND DISCUSSIONS

A. SIMULATION COMPARISON

To verify the effectiveness of the proposed method, the simulation model of the hybrid electric bus has been set up in the MATLAB platform, as shown in Fig. 17. The simulation model contains the hybrid powertrain model, the vehicle dynamics model, the control module, and etc. The simulation is executed on a computer with 8 GB RAM and 3.0 GHz of i5 processor, and the initial battery SOC is set at 0.55.

Fig. 18 illustrates a comparison of the simulation and reference velocities of the hybrid electric bus as determined by the CCBC cycle. As shown in Fig. 18, the deviation in the velocity is less than 3%, and it is indicated that the proposed method can maintain the velocity to the reference value over the entire cycle.

The simulation results over the CCBC cycle are shown in Fig. 19. Under low-speed driving conditions, the electric motor with the characteristics of a large torque output and fast response can provide the total drive torque for the bus running. With the assistance of the electric motor, the further optimization of the engine operation point becomes possible. As shown, the engine torque is basically greater than 200 N.m

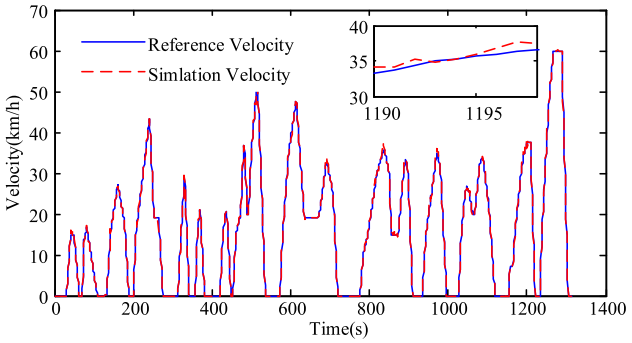

FIGURE 18. The simulation velocity over the CCBC cycle.

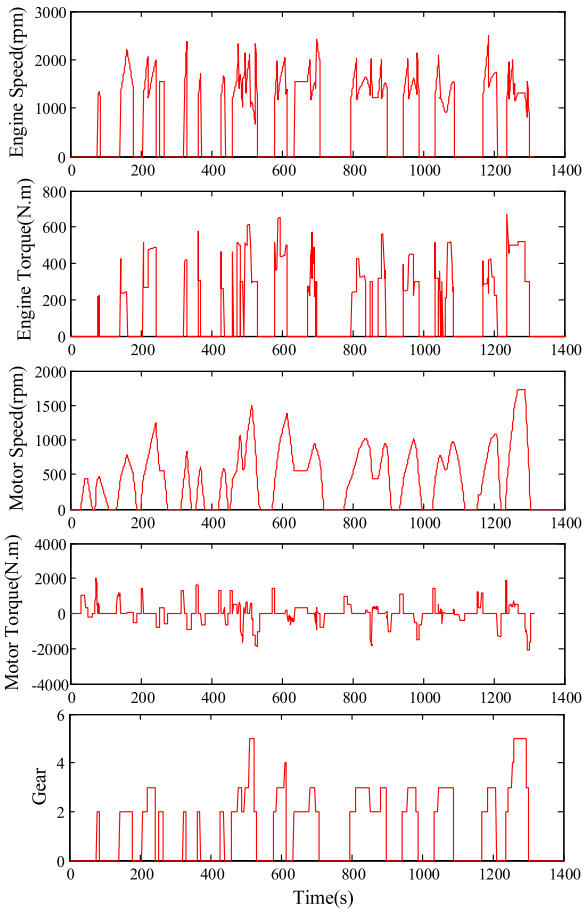

FIGURE 19. The results of the hybrid electric bus over CCBC cycle.

with the speed exceeding 1000 rpm, which means that engine operating points are almost distributed in the high-efficiency area. It is indicated that the engine only provides the power under a high load or highway driving conditions, which can result in greatly improved fuel economy. In addition, the electric motor can function as a generator to sustain the battery SOC level. Fig. 20 shows the battery SOC curve over the CCBC cycle with an initial value of 0.55. It is clear that the battery operates at a shallow cycle with small change in the battery SOC. Therefore, the battery will be maintained in a normal operating range without the formation of irreversible

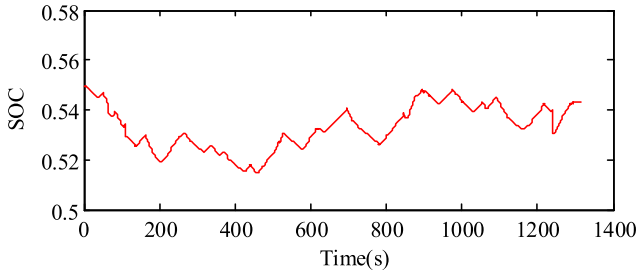

FIGURE 20. The curve of the battery SOC over the CCBC cycle.

damage, which is beneficial for improving the lifetime and reliability of the battery.

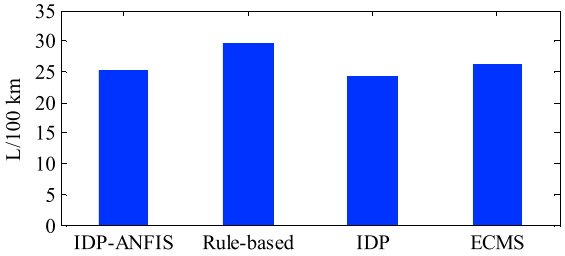

FIGURE 21. The comparison of the fuel economy over the CCBC cycle.

For analyzing the control performance of the proposed method, Fig. 21 provides the fuel consumption per hundred kilometers for the hybrid electric bus with different methods. IDP is chosen as the benchmark for the comparison. From Fig. 21, it is observed that the fuel economy obtained by the IDP-ANFIS, rule-based method, IDP and ECMS are 25.22 L/100 km, 29.67 L/100 km, 24.29 L/100 km, and 26.15 L/100 km, respectively. It is clear that the IDP obtains the lowest fuel consumption. However, this result is just the theoretically optimal value, which provides the empirical knowledge and evaluation criterion for other methods. Due to excellent reasoning and learning capabilities, the IDP-ANFIS is suitable to be utilized for the online control of hybrid electric bus. When compared to the optimum, the fuel consumption increment is approximately 3.83%. For the IDP-ANFIS, the offline training will miss several optimization values because of errors between the desired value and actual value. As for the ECMS, the fuel consumption is determined to a great extent by the equivalent factor. When compared to the IDP, the ECMS achieves 7.65% increase in fuel consumption. Furthermore, the rule-based EMS achieves the worst value regarding fuel economy. In short, for the EMS based on the IDP-ANFIS, the fuel consumption is much better than that of both the ECMS and rule-based methods.

Fig. 22 illustrates the emissions results with different methods over the CCBC cycle. It is observed from Fig. 22 that NO_x and CO production are the major pollutants expended into the air by the hybrid electric bus and have caused serious harm to the atmosphere. Since diesel engine always operate in oxygen-rich conditions, HC production is relatively low. For the IDP-ANFIS, the HC, CO and NO_x production values are

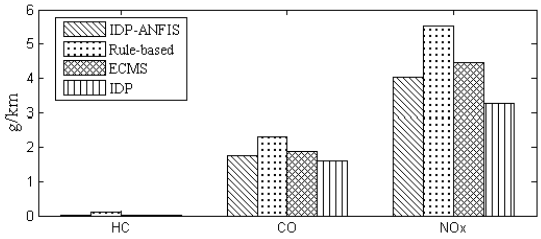

FIGURE 22. The comparison of emissions over the CCBC cycle.

0.009 g/km, 1.752 g/km, and 4.023 g/km, respectively. Likewise, the IDP-ANFIS achieves suboptimal emissions results over the CCBC cycle.

B. EXPERIMENTAL RESULTS

To validate the feasibility of the EMS based on the IDP-ANFIS, an experimental validation is carried out on the hybrid electric bus over the CCBC cycle. The aforementioned control strategy constructed in the MATLAB can be easily converted into C code using the Targetlink tools for the microcontroller programming. An exhaust acquisition device is directly connected to the exhaust pipes of the vehicle, as shown in Fig. 23(a). A freeway around the Yangcheng Lake is selected as the testing route, as shown in Fig. 23(b). The initial battery SOC is consistent with the simulation. The experimental results are illustrated in Fig. 24 and Table 6.

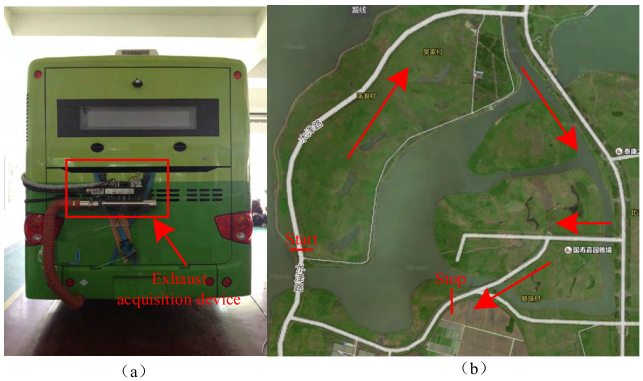

FIGURE 23. The arrangement of the experimental validation. (a) Exhaust acquisition device. (b) Testing route.

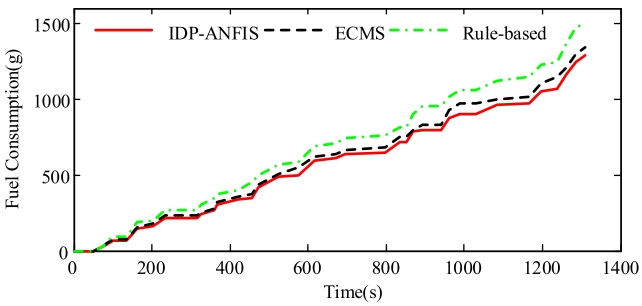

FIGURE 24. The fuel consumption curves over the CCBC cycle.

Even though the results do not exactly correspond with the simulation results, they present the advantage of the

TABLE 6. Experimental results for a comparison over the CCBC cycle.

Control strategy	Final SOC	Fuel Consumption		HC Production		CO Production		NO_x Production	
	---	L/100 km	Reduction	g/km	Reduction	g/km	Reduction	g/km	Reduction
Rule-based	0.550	30.51	--	0.0156	--	2.419	--	6.131	--
ECMS	0.552	27.29	10.55%	0.0139	10.89%	2.193	9.34%	5.872	4.22%
IDP-ANFIS	0.549	26.13	14.36%	0.0135	13.46%	2.112	12.69%	5.729	6.55%

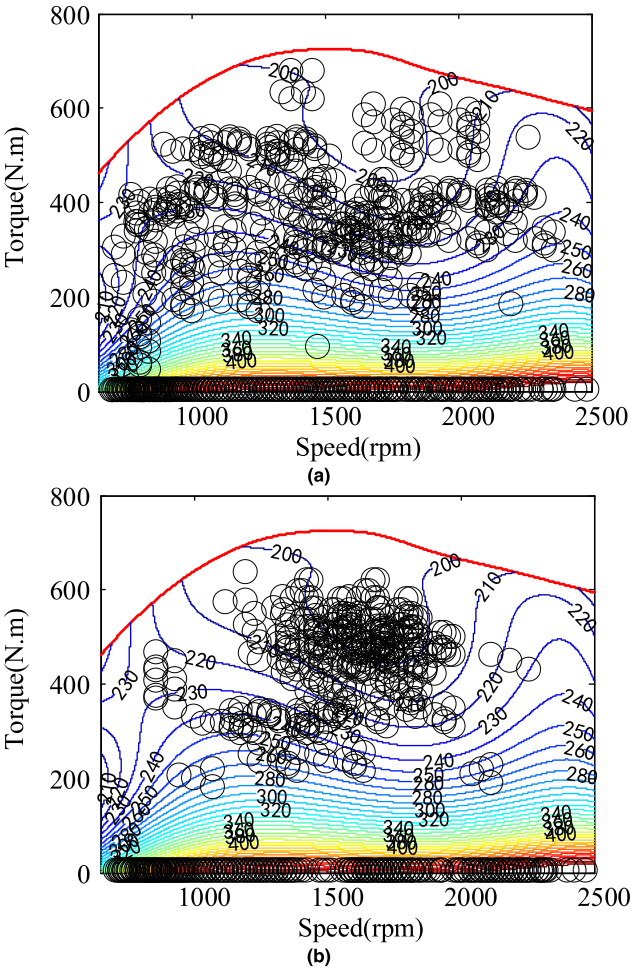

FIGURE 25. Engine operating points over the CCBC cycle. (a) Rule-based method. (b) IDP-ANFIS.

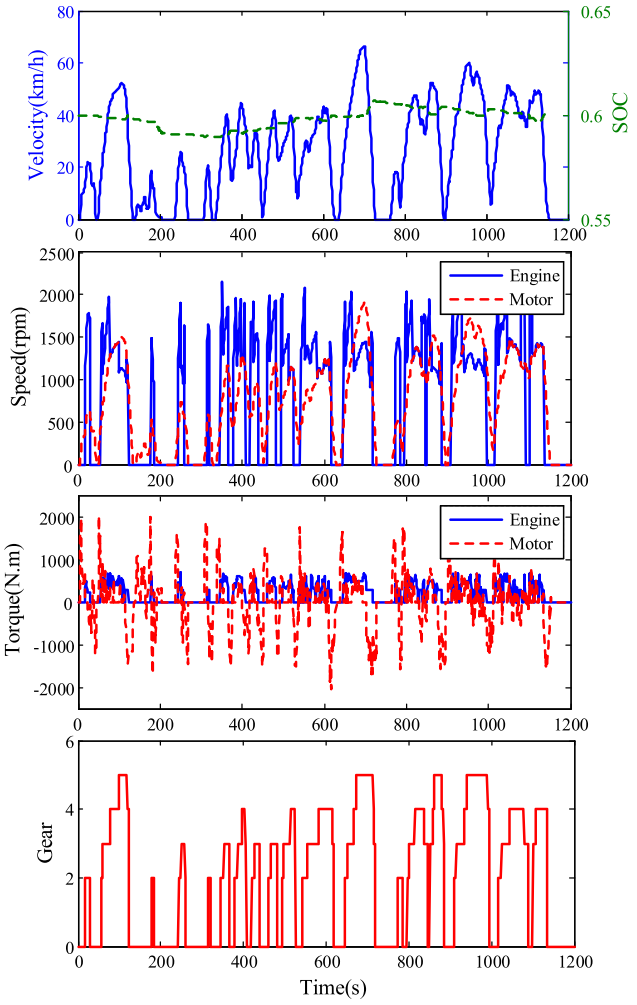

FIGURE 26. The results of the hybrid electric bus over C-WTVC cycle.

proposed method in comparison with other approaches. The deviation can be attributed to two aspects: one aspect is overlooking the instantaneous characteristic of the power sources and the other is due to model error. As shown in Fig. 24, the fuel consumption for the IDP-ANFIS is less than that of the ECMS and rule-based method. Compared with the rule-based method, for the ECMS, the reduction in the fuel consumption is approximately 10.55%. Because the control law produced by the ECMS based on an instantaneous state, the accuracy is not guaranteed. Nevertheless, the IDP-ANFIS achieves a 14.36% reduction in the fuel consumption. It is indicated that the IDP-ANFIS renders better decisions for the power distribution between the power sources, which fully utilize both chemical and electrical energy. The HC, CO, and NO_x production for the rule-based method, ECMS and IDP-ANFIS in units of gram per kilometer are described in Table 6. Compared with the rule-based method, the reduction in HC, CO, and NO_x are approximately 10.89%, 9.34%, and 4.22%, respectively, for ECMS results. Furthermore, the reduction in HC, CO, and NO_x for the IDP-ANFIS are 2.57%, 3.35%, and 2.33% higher than the reduction using the ECMS, respectively. It is demonstrated that the IDP-ANFIS can also effectively reduce the emissions of the hybrid electric bus to alleviate detrimental effects to the environment.

To further analyze why the proposed method can achieve better fuel economy, the engine operating points with two methods are drawn in Fig. 25. As shown, engine operating points in the high-efficiency area (b_e < 210 g/kW.h)

TABLE 7. Experimental results over the C-WTVC cycle.

Item	Rule-based	IDP-ANFIS	Reduction
Fuel consumption (L/100 km)	32.58	27.38	15.96%
HC (g/km)	0.0181	0.0146	19.33%
CO (g/km)	2.516	2.255	10.37%
NO_x (g/km)	6.457	5.988	7.26%

for rule-based method is approximately 20.8%. For the IDP-ANFIS, the distribution proportion of operating points is up to 45.1%. Consequently, it can be derived that the IDP-ANFIS can achieve better fuel economy than that of the rule-based method.

In addition, the proposed method is evaluated over a section of C-WTVC cycle (0∼1153s) to verify its effectiveness with respect to driving cycle changing. After training process, the multi-ANFIS with optimized parameters presents the sound control performance. The results are demonstrated in Fig. 26 and Table 7. The given velocity can be tracked strictly, and the zero SOC change is also achieved when the driving cycle is completed. Furthermore, the fuel economy, HC, CO and NO_x production of the proposed method can be reduced by 15.96%, 19.33%, 10.37% and 7.26% compared to that of the rule-based method, respectively.

VI. CONCLUSION

This paper presented an EMS based on the IDP-ANFIS with satisfied performance for a parallel hybrid electric bus running in city bus route. The optimal control trajectories over a specific driving cycle can be obtained by the IDP approach. The gear-shifting strategy was corrected by the FLC according to the vehicle acceleration and rate of change in the accelerator pedal, which combines both economic and dynamic gear-shifting strategies. Then, multi-ANFIS networks were designed and trained to learn the control law from optimal trajectories obtained before. The results of the simulations and experiments indicate that the control performance using the IDP-ANFIS-based EMS is better than that of both the ECMS and rule-based methods.

COMPETING INTERESTS

The authors declare that they have no competing interests.

REFERENCES

[1] X. Zeng *et al.*, "Predictive-model-based dynamic coordination control strategy for power-split hybrid electric bus," *Mech. Syst. Signal Process.*, vols. 60–61, pp. 785–798, Aug. 2015.
[2] C. Xia and C. Zhang, "Power management strategy of hybrid electric vehicles based on quadratic performance index," *Energies*, vol. 8, no. 11, pp. 12458–12473, 2015.
[3] J.-Y. Liang, J.-L. Zhang, X. Zhang, S.-F. Yuan, and C.-L. Yin, "Energy management strategy for a parallel hybrid electric vehicle equipped with a battery/ultra-capacitor hybrid energy storage system," *J. Zhejiang Univ. Sci. A*, vol. 14, no. 8, pp. 535–553, 2013.
[4] L. Serrao, S. Onori, and G. Rizzoni, "A comparative analysis of energy management strategies for hybrid electric vehicles," *ASME J. Dyn. Syst., Meas., Control*, vol. 133, no. 3, pp. 031012-1–031012-9, Mar. 2011.
[5] J. Hao, Z. Yu, Z. Zhao, P. Shen, and X. Zhan, "Optimization of key parameters of energy management strategy for hybrid electric vehicle using DIRECT algorithm," *Energies*, vol. 9, no. 12, p. 997, 2016.
[6] V. Sezer, M. Gokasan, and S. Bogosyan, "A novel ECMS and combined cost map approach for high-efficiency series hybrid electric vehicles," *IEEE Trans. Veh. Technol.*, vol. 60, no. 8, pp. 3557–3570, Oct. 2011.
[7] M. Montazeri-Gh and M. Mahmoodi-K, "Development a new power management strategy for power split hybrid electric vehicles," *Transp. Res. D, Transp. Environ.*, vol. 37, pp. 79–96, Jun. 2015.
[8] L. Li, X. Wang, R. Xiong, K. He, and X. Li, "AMT downshifting strategy design of HEV during regenerative braking process for energy conservation," *Appl. Energy*, vol. 183, pp. 914–925, Dec. 2016.
[9] X. Hu, N. Murgovski, L. Johannesson, and B. Egardt, "Energy efficiency analysis of a series plug-in hybrid electric bus with different energy management strategies and battery sizes," *Appl. Energy*, vol. 111, pp. 1001–1009, Nov. 2013.
[10] E. Silvas, T. Hofman, N. Murgovski, L. F. P. Etman, and M. Steinbuch, "Review of optimization strategies for system-level design in hybrid electric vehicles," *IEEE Trans. Veh. Technol.*, vol. 66, no. 1, pp. 57–70, Jan. 2017.
[11] T. Hofman, R. M. van Druten, A. F. A. Serrarens, and M. Steinbuch, "Rule-based energy management strategies for hybrid vehicles," *Int. J. Electr. Hybrid Veh.*, vol. 1, no. 1, pp. 71–94, 2007.
[12] H. Banvait, S. Anwar, and Y. Chen, "A rule-based energy management strategy for plug-in hybrid electric vehicle (PHEV)," in *Proc. Amer. Control Conf.*, Jun. 2009, pp. 3938–3943.
[13] M. H. Hajimiri and F. R. Salmasi, "A fuzzy energy management strategy for series hybrid electric vehicle with predictive control and durability extension of the battery," in *Proc. IEEE Conf. Electr. Hybrid Vehicles*, Dec. 2006, pp. 1–5.
[14] S. G. Li, S. M. Sharkh, F. C. Walsh, and C. N. Zhang, "Energy and battery management of a plug-in series hybrid electric vehicle using fuzzy logic," *IEEE Trans. Veh. Technol.*, vol. 60, no. 8, pp. 3571–3585, Oct. 2011.
[15] L. V. Pérez, G. R. Bossio, D. Moitre, and G. O. García, "Optimization of power management in an hybrid electric vehicle using dynamic programming," *Math. Comput. Simul.*, vol. 73, no. 1, pp. 244–254, 2006.
[16] D. Bianchi *et al.*, "A rule-based strategy for a series/parallel hybrid electric vehicle: An approach based on dynamic programming," in *Proc. ASME Dyn. Syst. Control Conf.*, Sep. 2010, pp. 1–8.
[17] C.-C. Lin, H. Peng, and J. W. Grizzle, "A stochastic control strategy for hybrid electric vehicles," in *Proc. Amer. Control Conf.*, vol. 5. Jun. 2004, pp. 4710–4715.
[18] G. Paganelli, S. Delprat, T. M. Guerra, J. Rimaux, and J. J. Santin, "Equivalent consumption minimization strategy for parallel hybrid powertrains," in *Proc. IEEE Veh. Technol. Conf.*, May 2002, pp. 2076–2081.
[19] J. Park and J.-H. Park, "Development of equivalent fuel consumption minimization strategy for hybrid electric vehicles," *Int. J. Autom. Technol.*, vol. 13, no. 5, pp. 835–843, 2012.
[20] C. M. Martinez, X. Hu, D. Cao, E. Velenis, B. Gao, and M. Wellers, "Energy management in plug-in hybrid electric vehicles: Recent progress and a connected vehicles perspective," *IEEE Trans. Veh. Technol.*, vol. 66, no. 6, pp. 4534–4549, Jun. 2017.
[21] C. Yang, S. Du, L. Li, S. You, Y. Yang, and Y. Zhao, "Adaptive real-time optimal energy management strategy based on equivalent factors optimization for plug-in hybrid electric vehicle," *Appl. Energy*, vol. 203, pp. 883–896, Oct. 2017.
[22] C. Musardo, G. Rizzoni, Y. Guezennec, and B. Staccia, "A-ECMS: An adaptive algorithm for hybrid electric vehicle energy management," *Eur. J. Control*, vol. 11, pp. 509–524, Jan. 2005.
[23] H. Borhan, A. Vahidi, A. M. Phillips, M. L. Kuang, I. V. Kolmanovsky, and S. Di Cairano, "MPC-based energy management of a power-split hybrid electric vehicle," *IEEE Trans. Control Syst. Technol.*, vol. 20, no. 3, pp. 593–603, May 2012.
[24] L. Li, C. Yang, Y. Zhang, L. Zhang, and J. Song, "Correctional DP-based energy management strategy of plug-in hybrid electric bus for city-bus route," *IEEE Trans. Veh. Technol.*, vol. 64, no. 7, pp. 2792–2803, Jul. 2015.
[25] L. Li, B. Yan, C. Yang, Y. Zhang, Z. Chen, and G. Jiang, "Application-oriented stochastic energy management for plug-in hybrid electric bus with AMT," *IEEE Trans. Veh. Technol.*, vol. 65, no. 6, pp. 4459–4470, Jun. 2016.
[26] A. Poursamad and M. Montazeri, "Design of genetic-fuzzy control strategy for parallel hybrid electric vehicles," *Control Eng. Pract.*, vol. 16, no. 7, pp. 861–873, Nov. 2008.

[27] R. Luus, "Piecewise linear continuous optimal control by iterative dynamic programming," *Ind. Eng. Chem. Res.*, vol. 32, no. 5, pp. 859–865, 1993.
[28] I. Yilmaz and O. Kaynar, "Multiple regression, ANN (RBF, MLP) and ANFIS models for prediction of swell potential of clayey soils," *Expert Syst. Appl.*, vol. 38, no. 5, pp. 5958–5966, 2011.
[29] Y. Lei, Z. He, Y. Zi, and Q. Hu, "Fault diagnosis of rotating machinery based on multiple ANFIS combination with gas," *Mech. Syst. Signal Process.*, vol. 21, no. 5, pp. 2280–2294, Jul. 2007.
[30] M. Buragohain and C. Mahanta, "A novel approach for ANFIS modelling based on full factorial design," *Appl. Soft Comput.*, vol. 8, no. 1, pp. 609–625, Jun. 2008.
[31] K. Salahshoor, M. Kordestani, and M. S. Khoshro, "Fault detection and diagnosis of an industrial steam turbine using fusion of SVM (support vector machine) and ANFIS (adaptive neuro-fuzzy inference system) classifiers," *Energy*, vol. 35, no. 12, pp. 5472–5482, Aug. 2010.
[32] X. Sun, B. Su, L. Chen, Z. Yang, X. Xu, and Z. Shi, "Precise control of a four degree-of-freedom permanent magnet biased active magnetic bearing system in a magnetically suspended direct-driven spindle using neural network inverse scheme," *Mech. Syst. Signal Process.*, vol. 88, pp. 36–48, May 2017.

XIANG TIAN was born in Zhenjiang, China, in 1983. He received the B.S. degree in electrical engineering and the M.S. degree in power electronics and power transmission from Jiangsu University, Zhenjiang, in 2006 and 2009, respectively, where he is currently pursuing the Ph.D. degree with the School of Automotive and Traffic Engineering.

His current research interests include electric vehicles, hybrid electric vehicles, parameter matching, optimal energy control strategy, and vehicle powertrain control.

REN HE was born in Nanjing, China, in 1962. He received the B.S. degree in vehicle engineering from the Jiangsu Engineering Institute, the M.S. degree in vehicle engineering from Jilin University, and the Ph.D. degree in power machinery and engineering (internal combustion engine) from the Jiangsu University of Science and Technology.

Since 1997, he has been a Professor and the Doctoral Supervisor with the School of Automotive and Traffic Engineering, Jiangsu University, where he is currently the Director of the Jiangsu Key Laboratory of Automotive Engineering. His research interests include the driving and braking theory and control technology for electric vehicles and hybrid electric vehicles and comprehensive energy saving technology for vehicles.

YIQIANG XU was born in Taixing, China, in 1991. He received the B.S. and M.S. degrees in vehicle engineering from Jiangsu University, Zhenjiang, China, in 2013 and 2016, respectively.

He is currently a System Engineer with the Suzhou Higer New Energy Automobile Electronic Control System Co., Ltd. His research interests include the advanced control strategies in vehicle powertrain systems and intelligent control.